JOURNAL OF PROPULSION AND POWER
Vol. 22, No. 1, January–February 2006

# Scramjet Lift, Thrust and Pitching-Moment Characteristics Measured in a Shock Tunnel

M. J. Robinson,* D. J. Mee,† and A. Paull‡
*The University of Queensland, Brisbane, Queensland 4072, Australia*

**Lift, pitching moment, and thrust/drag on a supersonic combustion ramjet were measured in the T4 free-piston shock tunnel using a three-component stress-wave force balance. The scramjet model was 0.567 m long and weighed approximately 6 kg. Combustion occurred at a nozzle-supply enthalpy of 3.3 MJ/kg and nozzle-supply pressure of 32 MPa at Mach 6.6 for equivalence ratios up to 1.4. The force coefficients varied approximately linearly with equivalence ratio. The location of the center of pressure changed by 10% of the chord of the model over the range of equivalence ratios tested. Lift and pitching-moment coefficients remained constant when the nozzle-supply enthalpy was increased to 4.9 MJ/kg at an equivalence ratio of 0.8, but the thrust coefficient decreased rapidly. When the nozzle-supply pressure was reduced at a nozzle-supply enthalpy of 3.3 MJ/kg and an equivalence ratio of 0.8, the combustion-generated increment of lift and thrust was maintained at 26 MPa, but disappeared at 16 MPa. Measured lift and thrust forces agreed well with calculations made using a simplified force prediction model, but the measured pitching moment substantially exceeded predictions. Choking occurred at nozzle-supply enthalpies of less than 3.0 MJ/kg with an equivalence ratio of 0.8. The tests failed to yield a positive thrust because of the skin-friction drag that accounted for up to 50% of the fuel-off drag.**

## Nomenclature

| | | |
|---|---|---|
| $C_L$ | = | coefficient of lift $2L/\rho v^2 S$ |
| $C_M$ | = | coefficient of moment $2m/\rho v^2 Sl$ |
| $C_T$ | = | coefficient of thrust $2F/\rho v^2 S$ |
| $F$ | = | thrust force |
| $g, \boldsymbol{G}$ | = | impulse response function or matrix |
| $H$ | = | enthalpy |
| $L$ | = | lift force |
| $l$ | = | chord length (=0.567 m) |
| $M$ | = | Mach number |
| $m$ | = | pitching moment |
| $P$ | = | pressure |
| $S$ | = | reference area ($=3.192 \times 10^{-3}$ m$^2$) |
| $T$ | = | temperature |
| $t$ | = | time |
| $u, \boldsymbol{u}$ | = | input function or vector |
| $v$ | = | velocity |
| $y, \boldsymbol{y}$ | = | output function or vector |
| $\gamma$ | = | ratio of specific heats |
| $\epsilon$ | = | strain vector |
| $\rho$ | = | density |
| $\Phi$ | = | equivalence ratio |

*Subscripts*

| | | |
|---|---|---|
| $A$ | = | axial direction |
| $a, b, c, d$ | = | stress bar A, B, C or D |
| $M$ | = | moment direction |
| $N$ | = | normal direction |
| $o$ | = | about leading edge of model |
| 0 | = | nozzle-supply condition |
| $\infty$ | = | freestream condition |

Received 6 February 2005; revision received 6 June 2005; accepted for publication 26 June 2005. 

*Graduate Student, Centre for Hypersonics, Division of Mechanical Engineering; currently Research Engineer, DLR, AS-RF, Bunsenstra$\beta$e 10, D-37073 Göttingen, Germany; matthew.robinson@dlr.de. Member AIAA.

†Associate Professor, Centre for Hypersonics, Division of Mechanical Engineering. Senior Member AIAA.

‡Research Professor, Centre for Hypersonics, Division of Mechanical Engineering. Member AIAA.

## Introduction

COST-EFFECTIVE space launch and hypersonic cruise vehicles are required for future research, industrial, and defense applications. This is likely to begin with the development of hypersonic cruise vehicles and to be followed with vehicles capable of accessing space. For both developments a propulsion system that is light, efficient, and cost effective is required. Airbreathing propulsion systems (such as scramjets and ramjets) offer such a technology.

However, the development of these propulsion systems is much more revolutionary in nature than previous propulsion developments, and thus severe technical challenges result.[1] For scramjet-powered vehicles, it is proposed that the engine be highly integrated with the vehicle. Thus, one of the challenges facing the designer is the control of body forces such as lift, thrust, and pitching moment when the engines are operating. To date, most research into hypersonic airbreathing propulsion has focused on optimization of engine thrust.

The importance of being able to quantify the effects of combustion on lift and/or pitching and yawing moments cannot be overstated in the overall design of operational hypersonic vehicles. For example, Engelund et al.[2] performed wind-tunnel tests on an unpowered model of the Hyper-X scramjet vehicle and made corrections for powered operation based on computational-fluid-dynamic (CFD) modeling. They predicted a substantial nose-down pitching-moment increment and a large increment in overall lift force in a powered-operation mode. This was because of pressurization of the aftbody nozzle surface area of the vehicle by the expanding exhaust flow. For trimmed flight at Mach 7 with the inlet closed, a 7-deg elevon deflection is predicted to be required. However, for powered operation, approximately no elevon deflection is predicted for trimmed operation at 2-deg angle of attack.

Therefore, the ability to make integrated force and moment measurements in ground-based testing facilities is seen as an important part of the design and development of airbreathing hypersonic systems. In the past, external airframe designs composed of body contours, lifting and control surfaces could be accomplished somewhat independently of the propulsion design and development. However, for supersonic and hypersonic flight vehicles that use designs with highly integrated engines and airframes, these interactions must be accounted for.

This paper reports measurements of the lift, thrust, and pitching moment on a scramjet model with variations in the mass flow rate of fuel, the simulated flight speed, and the freestream static pressure. A flexible force measurement system capable of measuring three components of force on multiple test models in the T4 Free Piston Shock Tunnel was developed to make the measurements. Measured forces are compared with forces calculated from a combined numerical and theoretical model of the scramjet.

Most force measurements on operating scramjet engines have been made in vitiated air blowdown facilities (e.g., Ref. 3), which typically have test times of order seconds so that conventional force measurement techniques can be used. The overall aerodynamic performance of fueled scramjet-integrated vehicles is sometimes estimated from separate component tests, theoretical analysis, or CFD calculations because of the limitations of the overall measurement capabilities (e.g., Refs. 4 and 5).

Between 1962 and 1978, scramjet-powered missile configurations were tested between Mach 4 and 10 for angles of attack up to 15 deg at the Johns Hopkins University.[6] Injector and combustor tests were carried out in direct-connect mode. Thrust measurements were made with the models attached to a sting arrangement that rides on a thrust balance carriage. Drag was balanced with thrust at an equivalence ratio of 0.5 in an optimized engine case.

Modular scramjet designs were tested in the combustion heated scramjet test facility at NASA Langley in the pre-National Aerospace Plane (NASP) period.[7] Up to six components of force were measured at simulated flight Mach numbers of 4 and 7 using load cells. Corrections to balance measurements were made for balance interactions, temperature effects, attitude tares, axes orientation, and pressure and momentum (flow) tares.

Mitani et al.[8] measured thrust, lift, and pitching moment on a side-compression engine at Mach 4 to 8 flight conditions in a vitiated-air facility at National Aerospace Laboratory (NAL). The model was suspended from a support strut with a diamond cross section on the axial-force measuring system. The model was designed to divide a support strut, two side walls, a cowl, and an engine strut, to itemize the individual drag forces by a strain-gauge load cell using a component buildup process. Integration of pressures measured on an identical model combined with allowance for skin-friction forces was used to compare calculated and measured forces. The drag forces agreed to within 5%. Two-thirds of the measured total drag was produced from the pressure and skin-frictional forces acting over the external surfaces of the model.

Kanda et al.[9,10] and Shimura et al.[11] tested a number of scramjet models at Mach numbers between 4 and 8 in the ramjet engine test facility at NAL. Up to three components of force (lift, thrust, and pitching moment) were measured using a floating frame force measurement system based on a number of load cells. To reduce vibrations and large loads associated with starting the tunnel, the model was initially locked during startup and then released to make measurements.[11]

Reproduction of hypersonic flight conditions above Mach 8 on the ground is usually restricted to impulse facilities with test times lasting only several milliseconds. These short test times preclude the use of conventional force-balance techniques for models of typical size,[12] and several alternative methods have been employed.[13–16] One technique, which has been shown to be quite suitable for force measurement in impulse facilities, is the stress-wave force measurement technique (SWFMT), originally proposed for single-component (drag) force measurement[17] and extended to multiple components.[18,19]

Measurements of force on scramjets in shock tunnels have been made in T4[20,21] and Hypulse[22] using stress-wave force balances and in HIEST[23] using an accelerometer-based balance. Paull et al.[20] used a single-component balance and measured a linear increase in incremental thrust force with equivalence ratio for equivalence ratios up to 0.90. The expected trend of decreasing thrust force with increasing nozzle-supply enthalpy was observed at a constant equivalence ratio of 0.77. Robinson et al.[22] showed that a three-component stress-wave force balance could be used to measure the forces generated by an operational scramjet engine in a shock tunnel but tests were only done for three flow conditions and two fuel flow rates. A three-component stress-wave force balance is used to measure forces on an operating scramjet for a range of conditions and fuel flow rates in the present paper.

## Stress-Wave Force Measurement Technique

The SWFMT involves measuring stress waves that propagate and reflect through the model and sting. Upon flow arrival, stress waves propagate through the model at the speed of sound of the material and subsequently enter a stress bar (or sting), which is instrumented with a strain gauge to record the time history of strain. If the system is linear, the resulting strain signal $y(t)$ can be related to the applied aerodynamic load $u(t)$ via an impulse response function $g(t)$, as described by the convolution integral,

$$y(t) = \int_0^t g(t-\tau)u(\tau)\,\mathrm{d}\tau \tag{1}$$

The aerodynamic force in an experiment can be determined by the deconvolution of the strain signal with the impulse response function. The impulse response function is determined usually through experiment[24] (as in this study) but can be obtained through finite element analysis (FEA).

A number of iterative deconvolution schemes exist for the solution of Eq. (1). In previous force measurement studies[19] the algorithm proposed by Prost and Goutte[25] has produced good results. The algorithm solves the discrete convolution equation using functional minimization with the extended conjugate gradient algorithm and is used exclusively in this paper.

Consider a three-dimensional system with input vectors $\boldsymbol{u}_N$, $\boldsymbol{u}_A$, and $\boldsymbol{u}_M$ and output vectors $\boldsymbol{y}_N$, $\boldsymbol{y}_A$, and $\boldsymbol{y}_M$. If the signals are discretized at time step $\Delta t$, the three output vectors can be related to the three input vectors by

$$\begin{pmatrix} \boldsymbol{y}_N \\ \boldsymbol{y}_A \\ \boldsymbol{y}_M \end{pmatrix} = \begin{bmatrix} \boldsymbol{G}_{\mathrm{NN}} & \boldsymbol{G}_{\mathrm{NA}} & \boldsymbol{G}_{\mathrm{NM}} \\ \boldsymbol{G}_{\mathrm{AN}} & \boldsymbol{G}_{\mathrm{AA}} & \boldsymbol{G}_{\mathrm{AM}} \\ \boldsymbol{G}_{\mathrm{MN}} & \boldsymbol{G}_{\mathrm{MA}} & \boldsymbol{G}_{\mathrm{MM}} \end{bmatrix} \begin{pmatrix} \boldsymbol{u}_N \\ \boldsymbol{u}_A \\ \boldsymbol{u}_M \end{pmatrix} \Delta t \tag{2}$$

Here, there are nine square submatrices relating each of the outputs to each of the inputs. Again, the impulse responses are found either experimentally or using finite element modeling. Multiple-component deconvolution is used to determine the three components of aerodynamic load from the three measured output signals.

## T4 Shock Tunnel and Test Conditions

### Facility

The T4 Free Piston Shock Tunnel is capable of simulating high-speed (suborbital) flows with varying Mach number. The current tests were performed at a compression ratio of 40 using the Mach 6 contoured nozzle and steel primary diaphragms from 2 to 4 mm thick. The nozzle had a throat diameter of 25.4 mm and an exit diameter of 265.0 mm.

### Test Conditions and Test Time

Tests were performed with a test gas of either air (for combustion) or nitrogen (to suppress combustion). The test conditions were calculated from the measurement of shock speed, nozzle-supply pressure, shock-tube filling pressure and temperature, and the ratio of pitot pressure in the test section to nozzle-supply pressure. The last quantity was not directly measured for all tests, and a nominal value of 0.012 was used. This is based on the pitot rake surveys of the Mach 6 nozzle by Overton and Mee[26] and corresponds to the mean value over the intake capture area of the scramjet model.

The freestream flow conditions were calculated using the computer programs ESTC,[27] NENZF,[28] and STN.[29] STN models the shock-tube flow and nozzle expansion for air in chemical equilibrium. It was used for nozzle-supply enthalpies less than 4.4 MJ/kg. ESTC was used to model the flow in the shock tube, and NENZF was used when the flow was expected to be in nonequilibrium and for the shots with nitrogen as the test gas.

The time for the nozzle flow to establish was determined by normalizing the pitot pressure by the nozzle-supply pressure, with an appropriate time delay to account for the time it takes the flow to pass from the nozzle-supply region to the pitot probe. For the Mach 6 nozzle at enthalpies between 3 and 5 MJ/kg, this was approximately 0.3 ms. Once the nozzle flow is established, it will take some time for the flow over the model to establish. A typical time for this is the time it takes for the mainstream flow to travel three model lengths.[30] This results in the beginning of the test window being approximately 0.9 ms after flow arrival for the current model length of 567 mm.

The end of the test window was set by either the time when the nozzle-supply pressure dropped 10% below the mean nozzle-supply pressure or by a 10% difference in the mean value of the ratio of nozzle-supply pressure to inlet pressure, measured at location PCB1 (see Fig. 1). (This difference is attributed to contamination of the test gas by the driver gas.) The end of the test window was usually set by the former criterion for tests at the higher nozzle-supply pressures ($\geq$32 MPa) and by the latter criterion for tests at lower nozzle-supply pressures.

The fuel equivalence ratio was varied at condition 4G (see Table 1). Condition 4G was chosen so that hydrogen would burn in the combustor. Conditions 3G and 2D were at the same nominal nozzle-supply enthalpy as for condition 4G but had lower nozzle-supply pressures. These conditions were used to investigate the influence of freestream pressure on the performance of the scramjet vehicle and are also summarized in Table 1. Shots were made at a large number of different conditions for the tests where the simulated flight speed was varied. Details for these conditions are given in Robinson.[31] Ninety-five-percent confidence level uncertainties in flow parameters are also given in Table 1. The freestream flow conditions were calculated for every shot, and shot-to-shot repeatability in the calculated freestream parameters was typically to within $\pm 3\%$.

**Table 1 Test conditions for conditions 4G, 3G, and 2D**

| Quantity | 4G | 3G | 2D | Uncertainty, % |
|---|---|---|---|---|
| $P_0$, MPa | 32.1 | 25.8 | 15.7 | —— |
| $H_0$, MJ/kg | 3.3 | 3.3 | 3.2 | —— |
| $v_\infty$, m/s | 2460 | 2440 | 2380 | 5 |
| $P_\infty$, kPa | 7.0 | 5.6 | 3.4 | 14 |
| $T_\infty$, K | 350 | 350 | 320 | 12 |
| $\rho_\infty$, kg/m$^3$ | 0.07 | 0.06 | 0.04 | 12 |
| $\gamma$ | 1.39 | 1.40 | 1.40 | 4 |
| $M_\infty$ | 6.6 | 6.6 | 6.6 | 5 |

## Model and Instrumentation

The aluminum scramjet body (see Fig. 1) was 567 mm long and composed of flat surfaces. The inlet surface was 73.8 mm wide and 179 mm long and had an inclination angle of 9.0 deg. The leading edge of the cowl was located 145 mm horizontally and 40.8 mm vertically from the leading edge of the scramjet. The shock wave formed by the inlet of the scramjet was not captured by the cowl at the Mach 6 conditions. The cowl was 5.0 mm thick and 257 mm long and had sharp leading and trailing edges. The internal surface of the leading edge of the cowl was inclined at 3 deg for the first 59 mm and the external surface at 15 deg for the first 7.5 mm. The internal surface of the trailing edge of the cowl had a 5-deg included angle.

Fuel was injected 104 mm from the leading edge of the inlet through five sonic orifices of 2.0 mm diam that spanned the width of the inlet. Injection from the inlet surface has been shown to be a viable means of delivering fuel to the combustor of a scramjet and can potentially reduce the required length of the combustor by allowing more time for the fuel to mix with air.[32] The injection angle was 45 deg to the inlet surface. The flow then entered a diverging combustion chamber of constant width and initial height of 10.0 mm. The combustion chamber was 162 mm long, and the final height was 11.0 mm. Flow was then expanded along the $-9.0$-deg inclined thrust surface for 144 mm. The final 86.2 mm of the thrust surface had a 3-deg included angle.

Stainless-steel swept side plates of 3.0 mm thickness prevented flow spillage. The cowl, side plates, and scramjet body were aligned with multiple dowel pins and held together using a high-strength bonding agent and multiple M5 and M3 countersunk screws.

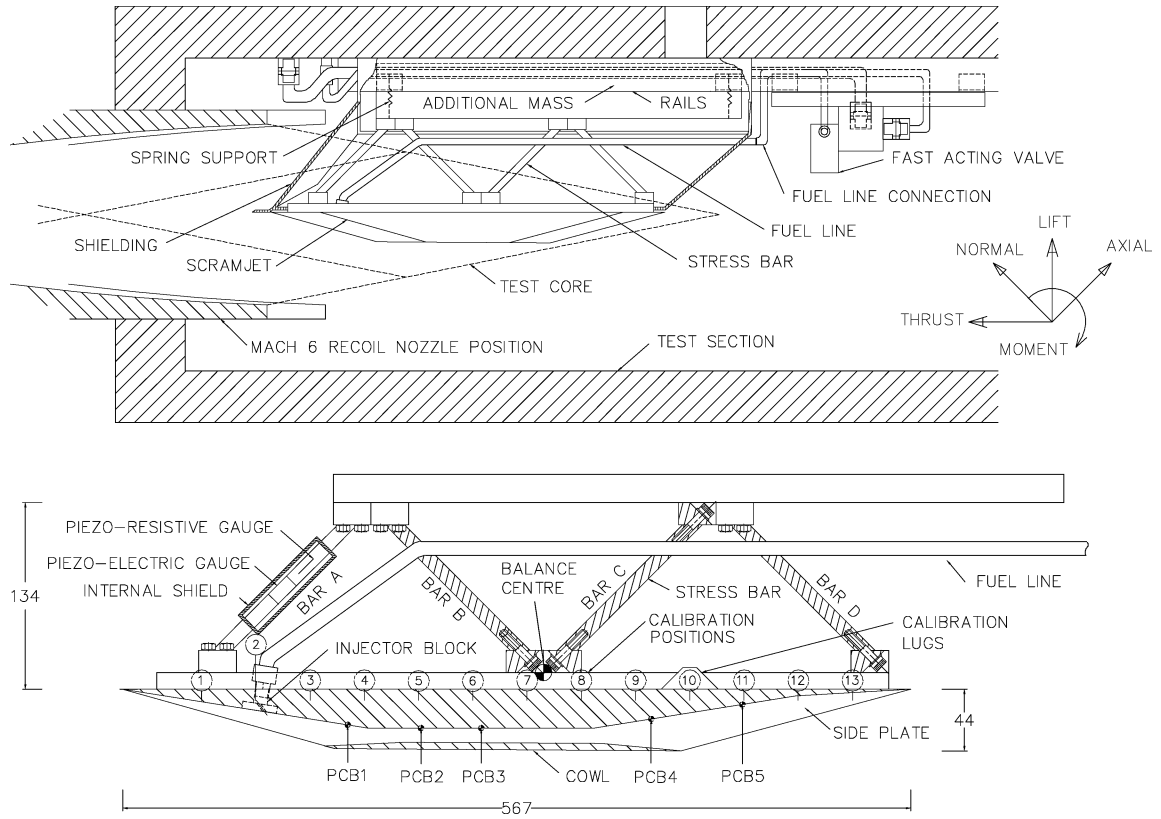


**Fig. 1 Experimental setup and scramjet model location in the test core (shielding for the fast acting valve is not shown). Dimensions in millimeters.**

Five PCB piezoelectric pressure transducers were used to measure static pressure down the centerline of the scramjet at locations 162.0, 215.0, 257.0, 379.0, and 446.0 mm from the leading edge of the inlet. One transducer was located on the inlet, two inside the combustion chamber and two along the thrust surface of the scramjet model.

The nozzle-supply pressure was measured using two PCB model 118A piezoelectric pressure transducers connected to charge amplifiers. The speed of the primary shock wave in the shock tube was determined from the timing of pressure rises measured by three piezoelectric pressure transducers nominally located at 2-m intervals. Pitot pressure was measured in the nozzle core flow for some tests using a PCB model 111A26 pressure transducer in a pitot probe. A PCB model 111A26 pressure transducer was used to measure the fuel pressure in the plenum chamber feeding the fuel-injection orifices.

The force balance, with the scramjet model attached, was suspended from the roof of the tunnel by springs to provide vibration isolation. Aerodynamic shielding was installed around the balance so that only aerodynamic forces on the scramjet vehicle were measured. This shielding (see Fig. 1) was rigidly mounted from the roof of the tunnel with a gap of approximately 2 mm between the bottom of the shielding and the top of the test model before the flow arrived. The model was free to move during the tests under the action of the aerodynamic loads, but movement was a maximum of several millimeters during the test time. The gap between the model and shielding allowed test gas to enter the shielding cavity during a test. The static pressure that built up inside the shielding applied a force to the shielded upper surface of the model. To obtain the correct values of force applied to the model (for comparison with the force predictions), this pressure was measured using two Kulite XCQ-080 pressure transducers.

Piezoelectric-film strain gauges[33] of size $25 \times 31$ mm were applied to each of the four stress bars of the force balance. Each gauge was sealed inside a 20-mm-diam, 80-mm-long section of PVC pipe to minimize pressure sensitivity of the gauges. Calibration of the force balance[24] for all tests was performed using a modally tuned PCB model 086C04 instrumented impact hammer.

Force coefficients were obtained by averaging the force signals during the test time and dividing the result by the average value of $\frac{1}{2}\rho_\infty v_\infty^2 S$ during the test time. The length scale used for the pitching-moment coefficient was the chord length of the model ($l = 0.567$ m). The pitching-moment coefficient is defined about the balance center that was located 300 mm in the thrust direction and 12 mm in the lift direction, from the leading edge of the scramjet.

An uncertainty analysis of the measured forces and force coefficients was made. Contributions to the uncertainties in the measurement of aerodynamic forces were considered from uncertainties in the calibration of the balance, noise induced on the strain signals caused by the transmission of vibrations from the tunnel to the balance, errors in data acquisition, errors in the deconvolution process to infer aerodynamic forces from the measured strain signals, and errors caused by the buildup of pressure inside the shielding. Ninety-five-percent confidence-limit uncertainties in the measured values of lift and thrust forces are estimated to be $\pm 7$ and $\pm 4\%$ of the resultant force on the model, respectively. The uncertainty in the measured center of pressure is $\pm 1\%$ of the model chord. There are additional uncertainties in the force coefficients caused by uncertainties in the freestream conditions. The overall uncertainties for the experimentally measured coefficients of lift, thrust, and pitching moment for cases with no fuel injection are $\pm 10$, $\pm 7$, and $\pm 17\%$, respectively. Typical values for the cases with fuel injection are $\pm 9$, $\pm 7$, and $\pm 10\%$, respectively. The larger uncertainty in pitching-moment coefficient for the case of no injection arises because the line of action of the resultant force is closer to the center of the balance for that case. Full details of the uncertainty analysis and the experimental arrangement are given in Robinson.[31]

#### Fuel Ejection into a Vacuum

The fuel-injection system was calibrated by ejecting hydrogen when there was no test flow, and the model was installed in the evacuated test section. By knowing the initial and final pressures in the fuel reservoir and the time history of pressure in the injection plenum chamber, the mass flow rate of fuel as a function of the injection pressure was determined. The forces on the model during injection could also be found by deconvolving the signals recorded from the stress bars during the fuel calibration tests. The resulting forces are plotted as a function of the pressure in the injection plenum chamber in Fig. 2. The measured forces vary approximately linearly with pressure. Note that the streamwise force is plotted as drag in this figure. The negative values indicate that the ejection of hydrogen produced a thrust on the model.

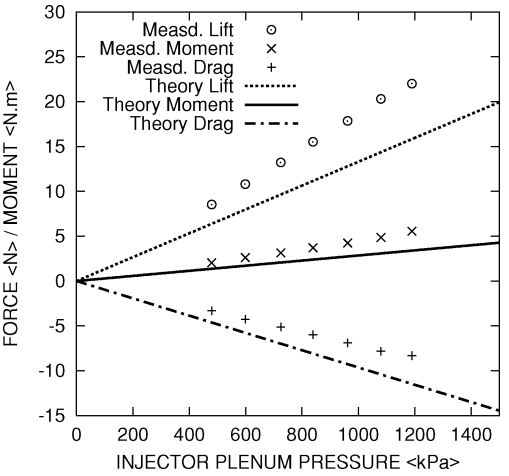


**Fig. 2 Forces for fuel injection into a vacuum—measured and theoretical.**

In effect, the fuel calibration tests are those for a cold-jet thrustor. The force on the model as a result of the momentum of the fuel jet was calculated from the mass flow rate of fuel by assuming that the flow at the exit of the fuel-injection holes was choked. The thrust and lift forces and the pitching moment caused by ejection were then calculated from the angles and locations of the fuel-injection holes. The forces calculated vary linearly with the pressure in the injection plenum chamber and are shown by the straight lines in Fig. 2. It can be seen that there are some small differences between the calculated and the measured forces. The differences are attributed to stresses induced in the flexible fuel line feeding the injector when the fast-acting fuel valve opens and the line is pressurized. In processing the results from the experiments, the forces caused by these stresses are taken to be the differences between the measured and theoretical forces shown in Fig. 2.

## Force Balance Design

Dynamic FEA can be used to simulate the performance and assess accuracy of force balance designs.[19,22,34] The FEA interface package used here was MSC/PATRAN (which served as a pre- and postprocessor), and the solver package used was MSC/NASTRAN. In general, solid HEX8 and WEDGE6 elements were used. No nodes were fixed for the final simulation; however, the large inertial mass was connected to grounded springs of stiffness 5 kN/m. Direct integration with an implicit technique based on the Newmark method was employed. Several design configurations were investigated, and the final design and the coordinate system are shown in Fig. 1.

In the experiments, the balance was calibrated by measuring its response to point loads applied at a set of locations on the model. The aerodynamic loads on the model in a shot of the tunnel are caused by pressure and skin-friction forces distributed over all of the model's surfaces. This distribution changes as the fuel flow rate and flow conditions change. Figure 3 shows examples of the loading distributions for fuel-off and fuel-on conditions estimated from CFD simulations for condition 4G made using the two-dimensional space-marching code SM3D.[35] FEA was used to assess whether the overall aerodynamic forces on the scramjet model could be determined using an impulse response for the balance determined from a set of point calibration loads.

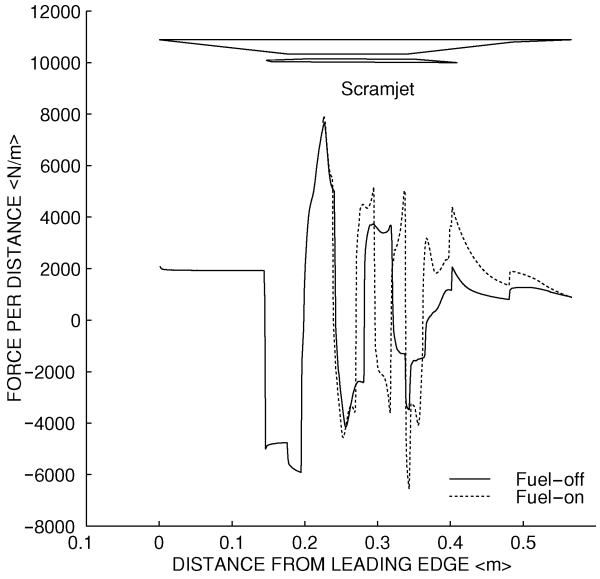


**a) Lift distribution**

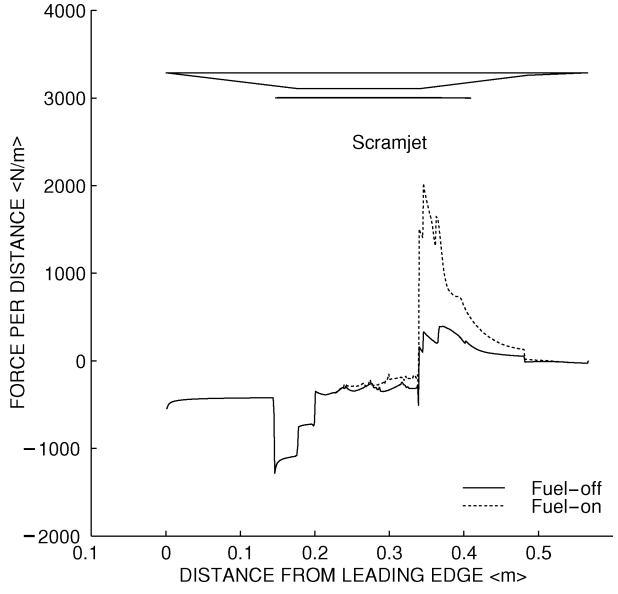


**b) Thrust distribution**

**Fig. 3 CFD loading distributions for fuel off and fuel on ($\Phi = 0.85$).**

Simulated calibration loads were applied directly to the top surface of the FEA model of the scramjet. In total, 26 test cases were solved. Step point loads of lift and thrust were applied separately at each of 13 locations (see locations identified as 1 to 13 in Fig. 1). For each case, the strain was monitored at locations on the FEA model corresponding to the location of the strain gauge on each of the four stress bars. This produced 104 strain signals. The strain signals from the four bars for each test case were combined to produce three output signals in the form

$$\boldsymbol{y}_N = \epsilon_b + \epsilon_d, \qquad \boldsymbol{y}_A = \epsilon_a + \epsilon_c \qquad \text{and}$$

$$\boldsymbol{y}_M = \epsilon_a - \epsilon_c + \epsilon_b - \epsilon_d \tag{3}$$

This reduced the number of signals to 78. The responses of each of the three outputs, $\boldsymbol{y}_A$, $\boldsymbol{y}_N$, and $\boldsymbol{y}_M$, to step inputs of unit lift, thrust, and pitching moment were found by superposition of scaled combinations of these 78 responses. Scaling factors were chosen so that the net loading was similar in distribution to the fuel-off loading shown in Fig. 3. This produced nine unit step responses. These were numerically differentiated with respect to time[24] to produce the nine impulse response submatrices in Eq. (2). The final combined impulse response matrix is referred to as the "global" impulse response function.

Two simulated pressure and skin-friction loads were then applied to surfaces of the FEA model. One case was for the fuel-off loading and the other for the fuel-on loading shown in Fig. 3. Note that forces caused by fuel injection were not included in the loads. For each case the time history of loading was set to represent that expected in a shot of the tunnel. Skin friction was applied by using multiple point loads on the inlet, combustion chamber, thrust surface, internal and external surfaces of the side plates, and also the cowl.

The strain signals for the four stress bars from the simulations were combined according to Eq. (3) and were deconvolved using the global impulse response function. Results are shown in Fig. 4. It can be seen that the recovered signals follow the applied loads quite well. The force signals were averaged from 2.0 to 4.5 ms to quantify how well the loads were recovered. Relative errors of

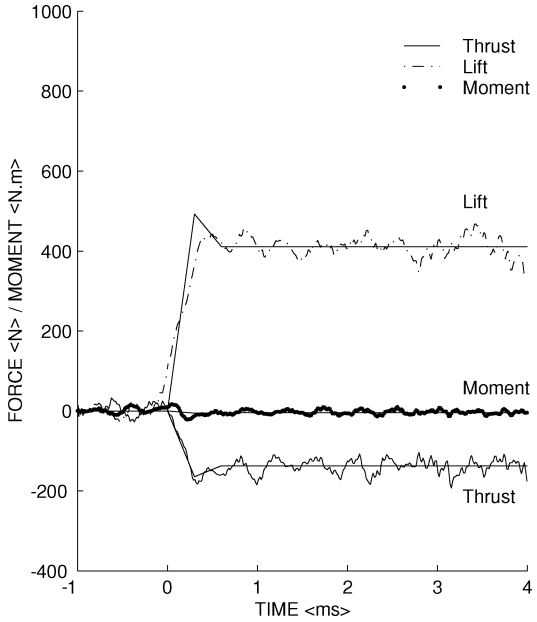


**a) Fuel-off tunnel recovered loads**

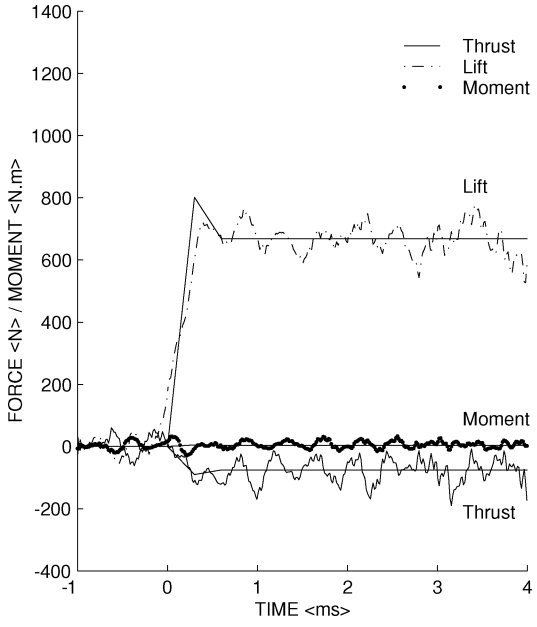


**b) Fuel-on tunnel recovered loads**

**Fig. 4 Applied (smooth lines) and recovered (jagged lines) loadings for simulated fuel-off and fuel-on conditions obtained by deconvolution using the global fuel-off impulse response function. The modeled flow arrival is at $t = 0$ ms.**

less than 1.5% for the recovered forces and less than 1.0% for the center of pressure as a percentage of chord were obtained for the fuel-off case. Similar errors were obtained for the recovered fuel-on tunnel loadings but with a slightly higher error of 2.5% on the thrust component. These results were taken as a validation of the proposed procedures for calibration and operation of the balance and were used to help quantify uncertainties in the experimental measurements.

## Force Prediction

The forces acting on the scramjet were modeled using a combination of computational and theoretical analyses. The purpose of the modeling was to check the reliability of the force coefficients indicated by the balance for varying fuel flow rates and flow conditions. Several simplifying assumptions were made, including estimating the heat release of combustion from measured pressures and neglecting three-dimensional effects. The approach to modeling is similar to that used in Robinson et al.,[22] and so only a summary is given here.

### Numerical Component

The numerical parts of the force predictions were made using the two-dimensional space-marching code SM3D.[35] This was used to make a two-dimensional model of the internal flow path of the scramjet. The flow on the outer surface of the cowl was simulated separately on a separate grid, also using SM3D. A grid size of 32,000 (in the thrust direction) by 320 (in the lift direction) was used for simulating both regions. Overall pressure and skin-friction forces were calculated. Forces on all other surfaces, including those on all side walls of the vehicle, were modeled using simple hypersonic theory.

The gas model was ideal air or ideal nitrogen. The flow was modeled as fully viscous and turbulent using the Baldwin–Lomax model.[36] The temperature of the walls was set at 290 K.

For simulations at fill condition 4G, the oblique shock generated at the leading edge of the inlet is not captured by the cowl, and the average pressure and temperature at the entrance to the combustor are 100 kPa and 900 K, respectively. These conditions should be suitable for hydrogen combustion.[37] Combustion was simulated by addition of thermal energy in the source term of the energy equation. This energy was evenly distributed over the length of the combustion chamber in the simulations. Some calculations were made with other distributions of heat release, and results were used to determine the uncertainty in the force prediction model caused by uncertainty in the distribution of heat release.

Data from the experiments were used to determine the amount of heat to be added in the simulations. The heat release was adjusted until the simulated and measured pressures at the locations of first two pressure transducers on the thrust surface were matched.

A mesh-refinement study was performed for the simulation at condition 4G with no heat addition. Meshes of sizes $8000 \times 80$, $16000 \times 160$, and $32000 \times 320$ were tested. For the mesh-refinement study, the same mesh scaling parameters, boundary conditions, time steps, computational flow models, numerical stability, and convergence criteria were used. Richardson extrapolation[38] was used to determine the fractional error for each force. The error in lift force was 1%, that in thrust force was 5%, and that in pitching moment was 2%. The larger error in the thrust component is caused by the relatively large contribution of skin friction and the degree to which the boundary layers could be resolved. All subsequent simulations were done using the finest grid.

The results from the two-dimensional numerical simulations were also used to estimate the viscous forces on the inner side walls of the scramjet vehicle. For the inlet side walls, the total viscous force computed on the two-dimensional inlet surface was averaged over its area. This average value was multiplied by the area of the side walls of the inlet to obtain an estimate of the skin-frictional force acting on inner surfaces of these side walls. This force included components in both lift and thrust directions. A similar procedure was used for the inner side walls of the combustor and the thrust surface. For the combustor, the area-averaged viscous force was based on the mean values computed for the upper and lower surfaces of the combustor.

### Analytical Component

The scramjet is of a simple design in that the vehicle is composed of two-dimensional surfaces. This allows simple hypersonic theory and boundary-layer calculations to be used to determine aerodynamic forces on surfaces not included in the computational simulations.

The forces on the bevelled leading and trailing edges of the side walls were taken into account in the modeling. Oblique shock-wave theory and Prandtl–Meyer expansion theory were used to calculate the forces acting on these and on the external side walls of the scramjet vehicle.

Viscous forces on the external surfaces were calculated using flat-plate, zero-pressure-gradient approximations. A reference temperature method, with Eckert's reference temperature,[39] was used to calculate frictional forces on surfaces where the boundary layer was assumed to be laminar. Transition from laminar to turbulent flow was taken to occur when the Reynolds number, based on distance from the effective origin of the laminar boundary layer, was greater than $2 \times 10^6$. This value is based on boundary-layer transition studies in the T4 Free Piston Shock Tunnel.[40] The theory of Spalding and Chi[41] was used to calculate the forces caused by turbulent skin friction.

As noted earlier, there will be some force on the model as a result of the momentum of the ejected hydrogen. The method used to calculate this force is described in the section entitled "Model and Instrumentation."

## Experimental Results

### Force Measurements

Two corrections were made to the direct force measurements determined from the balance. The effects of stresses in the fuel lines were removed using the results in Fig. 2. The force applied to the scramjet model from the buildup of pressure within the internal shielding cavity was removed from the measured lift force and pitching moment using the pressure measured in the cavity. This pressure does not affect the thrust because the scramjet model was tested with no angle of attack.

An example of the forces measured in a shot at condition 4G for no fuel injection is shown in Fig. 5a. This shows the directly measured and corrected signals. A 500-$\mu$s moving average was applied to the recovered signals. The uncorrected lift drops as the pressure in the cavity increases during the test. However, the corrected signal remains approximately steady during the test period. The negative thrust signal indicates drag.

When fuel was injected, the fuel valve was typically opened at least 10 ms before flow arrival to ensure a steady fuel pressure during the test period. An example of forces for a shot at condition 4G with fuel injection is shown in Fig. 5b. Prior to flow arrival, the nonzero signals result from the forces caused by injection. These are small on the scales used in the plot (e.g., lift force caused by fuel injection is approximately 20 N). It can be seen that there are increases in lift and thrust over the levels measured without injection. This is associated with combustion of the fuel. Again, the corrected lift and thrust forces are approximately constant during the test time. The rapid changes in forces beyond about 4 ms after flow arrival are a result of the model moving far enough to strike the shielding. (Recall that the model and force balance are suspended and are free to move.) Results from any shots in which this occurred before the end of the test period were discarded. The moment and uncorrected moment signals are indistinguishable for the fuel-off case and prior to the shielding strike for the fuel-on case. The force coefficients presented in this paper are based on the corrected signals.

### Variation of Equivalence Ratio

Tests were performed at condition 4G to investigate the effect of variations in equivalence ratio on the performance of the scramjet. The simulated flight speed and freestream pressure were kept

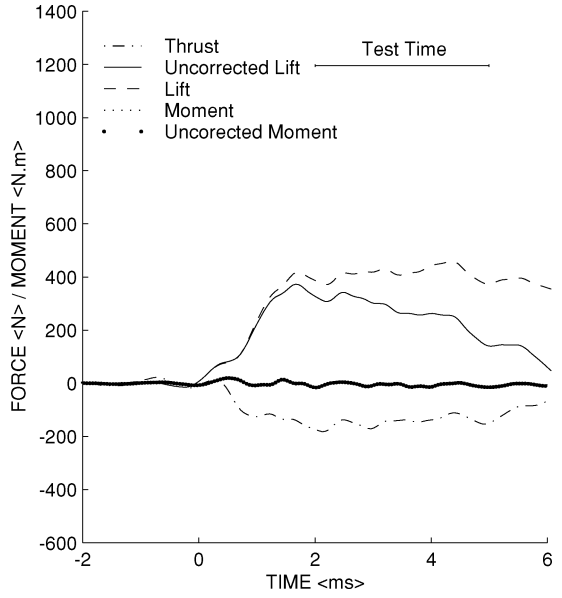


**a) Shot 7413—no fuel**

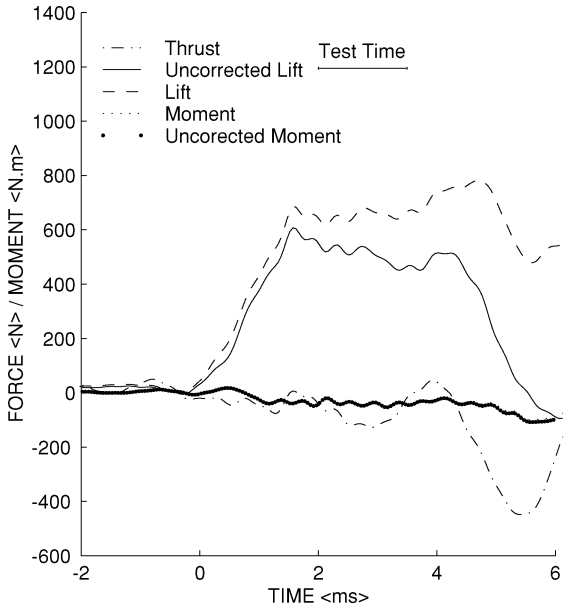


**b) Shot 7416 Φ = 1.0**

**Fig. 5 Typical force signals. Condition 4G. Flow arrival is at $t = 0$ ms. 500-$\mu$s moving average applied to recovered loads.**

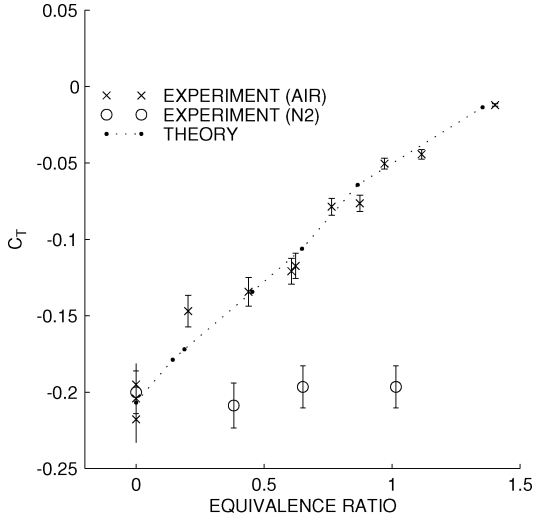


**Fig. 6 Coefficient of thrust at various equivalence ratios for condition 4G.**

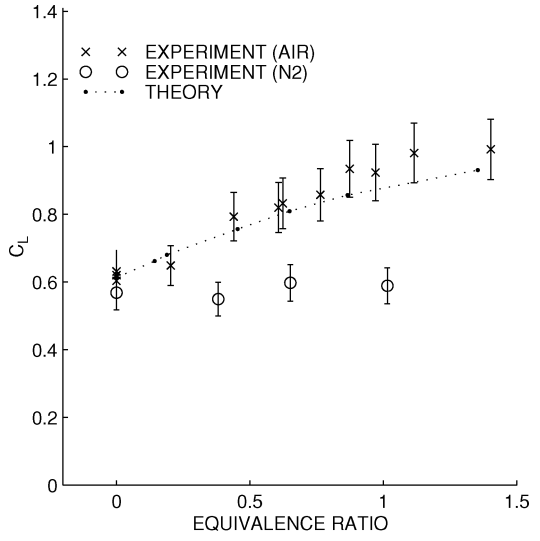


**Fig. 7 Coefficient of lift at various equivalence ratios for condition 4G.**

constant while the equivalence ratio was varied from 0.0 to 1.4. Shots were done in both air and nitrogen test flows.

The measured thrust coefficients are shown in Fig. 6. The uncertainty in equivalence ratio was $\pm 17\%$, but, for clarity, error bars for $\Phi$ are not shown in this or subsequent plots. The thrust coefficient is approximately $-0.21$ for no injection. When fuel was injected, the thrust coefficient increased approximately linearly with equivalence ratio. The theoretical thrust coefficients are in good agreement with those measured. Note that experimentally measured pressures on the thrust surface were used to help to estimate the heat release in the combustion model of the theoretical analysis. In the absence of combustion (shots with nitrogen as the test gas), the thrust coefficient remained approximately constant as the mass flow rate of hydrogen increased. Thus, the increase in thrust for the air shots was caused by combustion of the fuel. Even at the highest equivalence ratio, the thrust produced by combustion was just insufficient to balance the drag. The theoretical modeling indicated that skin-frictional forces accounted for up to 50% of the total fuel-off drag. This highlights the importance of methods for skin-friction reduction, such as boundary-layer combustion,[42] for development of operational scramjet-powered vehicles.

The corresponding lift coefficients are shown in Fig. 7. The lift coefficient increased by approximately 50% when the equivalence ratio was increased from 0 to 1, showing the strong coupling between engine operation and aerodynamic characteristics for such an engine-integrated vehicle. The lift force coefficient increased approximately linearly with equivalence ratio until an equivalence ratio of one. Linear variations in lift and thrust coefficients with equivalence ratio were also obtained by Kanda et al.[9] Paull et al.[20] also measured a linear increase in thrust with equivalence ratio. The lift coefficients for tests in which fuel was injected into a nitrogen flow were similar to those for the tests with no fuel injection and air as the test gas. The lift coefficient continued to increase for equivalence ratios in excess of 1, albeit at a lower rate than for lower equivalence ratios. The continued increase in thrust and lift coefficients for equivalence ratios in excess of unity are larger than can be accounted for by increased thrust from injection alone. This indicates that there was additional heat release from combustion for equivalence ratios in excess of unity in this scramjet at condition 4G.

The measured and predicted pitching-moment coefficients for condition 4G are shown in Fig. 8. The increasingly negative measured pitching-moment coefficient obtained as the fuel flow rate was increased corresponds to an increasing nose-down pitching moment

**Table 2 Comparison between predicted and experimental force coefficients at condition 4G; $\Phi = 0.0$**

| Quantity | Theory | Experiment | % Error |
|---|---|---|---|
| $C_L$ | 0.61 | 0.62 | 1.6 |
| $C_T$ | −0.21 | −0.21 | 0.0 |
| $C_{Mo}$ | −0.34 | −0.32 | −5.9 |

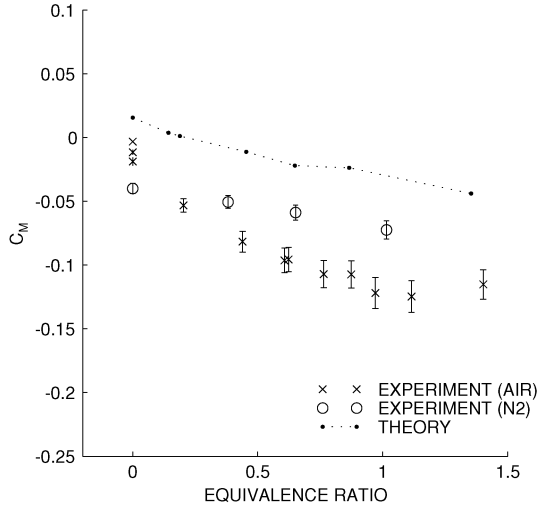


**Fig. 8 Pitching-moment coefficient at various equivalence ratios for condition 4G.**

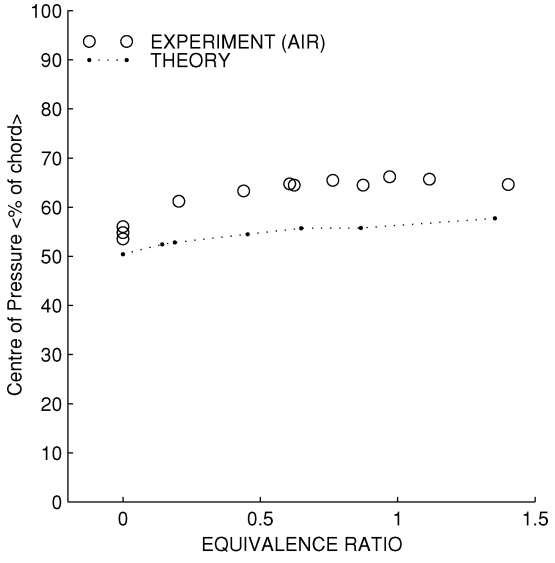


**Fig. 9 Center of pressures at various equivalence ratios for condition 4G.**

on the vehicle. The corresponding shift in center of pressure is shown in Fig. 9. A shift of approximately 10% was measured as the equivalence ratio increased from 0 to 1. The center of pressure varied by less than 3% in the range of $0.8 < \Phi < 1.2$.

The measured fuel-off force coefficients at condition 4G (averaged over three shots) are compared with the theoretical values in Table 2. Good agreement for lift and drag coefficients was obtained, but the agreement for pitching-moment coefficient was poorer. As the fuel flow rate increased, the theoretical pitching-moment coefficient shows a similar trend to that measured, but the discrepancy remains. The poor agreement for the pitching-moment coefficient is attributed to the difficulty in accurately predicting the pressure distribution on the latter parts of the thrust surface. Several approximations were made to simplify the force prediction calculations. For example, the modeling did not include any interaction between the test flow over the cowl and the flow exiting the combustion chamber. Any errors in the pressures towards the end of the thrust surface have a relatively large influence on pitching moment because of the large moment arm for the associated forces. Therefore, errors in that region do not affect the lift and thrust forces to the same degree that they affect pitching moment. This highlights the importance of accurately modeling the flow through the engine for the prediction of pitching-moment characteristics in engine-integrated scramjet vehicles.

The results for the tests at condition 4G in which hydrogen was injected into a nitrogen test flow also show a small change in pitching moment for increased injection flow rates. This contrasts with the thrust and lift coefficients that remained approximately constant as the fuel flow rate increased. This might be because of changes in the wave patterns through the scramjet resulting from interaction of the hydrogen jet and the influence this has on the distribution of pressures on the thrust surface.

### Variation of Simulated Flight Speed

Tests were also performed to investigate the influence of flow speed on the performance of the scramjet. The nozzle-supply enthalpy of the flow was varied from 3 to 5 MJ/kg (equivalent flight Mach numbers from 8.1 to 10.5) at a nominal nozzle-supply pressure of 32 MPa. Shots with air as the test gas were done with fuel injection at $\Phi = 0.8 \pm 0.10$ and without fuel injection. Shots were also done with fuel injection into a nitrogen test flow.

The variation of thrust coefficient with nozzle-supply enthalpy is shown in Fig. 10. The thrust coefficient for the fuel-off shots (labeled "TARE") varied by less than ±7% over this range of conditions. As expected, the thrust coefficient for the fueled shots decreased as the enthalpy increased. There was a 75% reduction in drag at the lowest enthalpy condition, but this decreased to only a 20% reduction at the highest enthalpy condition tested.

The lift coefficients are shown in Fig. 11. The lift coefficients measured for the tare shots are constant to within the measurement uncertainty limits. The levels for shots in which hydrogen was injected into a nitrogen test flow are similar. The increase in lift coefficient for the shots in which hydrogen was injected into an air test flow is approximately uniform over the range of enthalpies tested with a typical increase of approximately 50%.

The pitching-moment coefficient for the injection of fuel into an air test gas remained approximately constant over the range of nozzle-supply enthalpies tested, although there was a slight increase in the measured pitching moment at high enthalpies (a larger pitch-down moment coefficient). This resulted in negligible change in center of pressure with increasing enthalpy because the lift coefficient for this fuel equivalence ratio also remained approximately constant with increasing enthalpy.

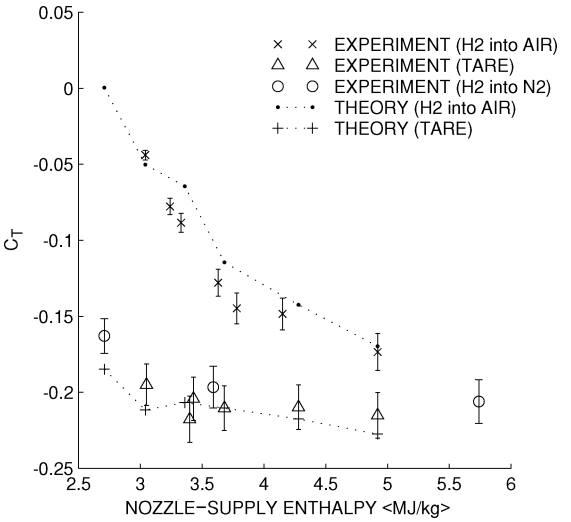


**Fig. 10 Coefficient of thrust at $\Phi = 0.00$ and 0.80 (nom.) for various nozzle-supply enthalpies.**

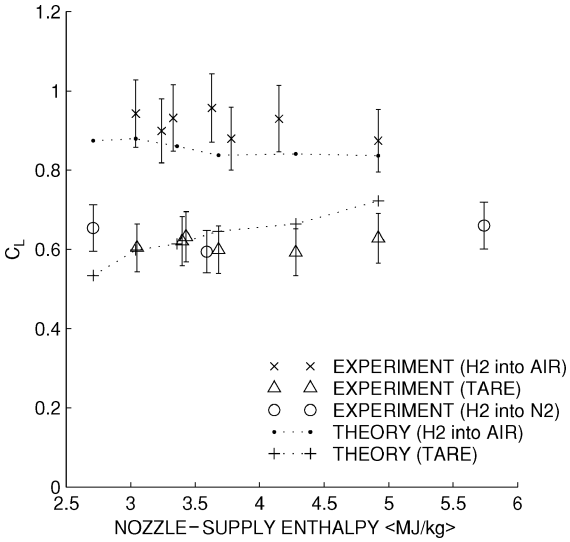


**Fig. 11 Coefficient of lift at $\Phi = 0.00$ and 0.80 (nom.) for various nozzle-supply enthalpies.**

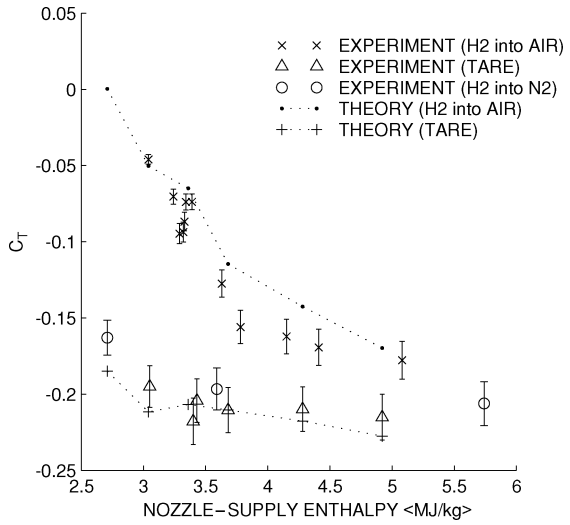


**Fig. 12 Coefficient of thrust at $\Phi = 0.00$ and 0.80 (nom.) for various nozzle-supply enthalpies. Additional data after $\Phi$ correction.**

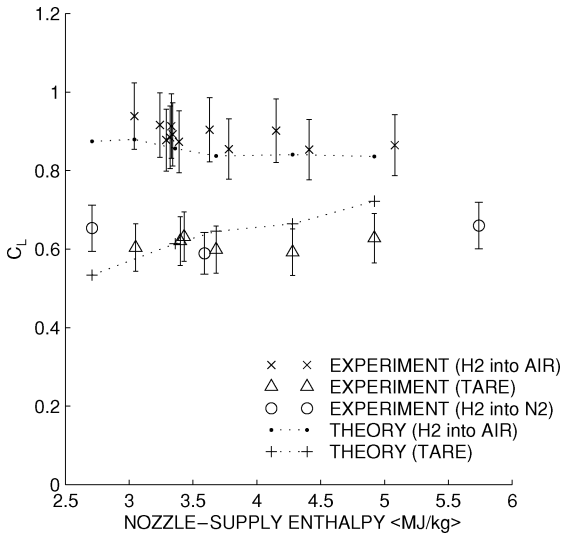


**Fig. 13 Coefficient of lift at $\Phi = 0.00$ and 0.80 (nom.) for various nozzle-supply enthalpies. Additional data after $\Phi$ correction.**

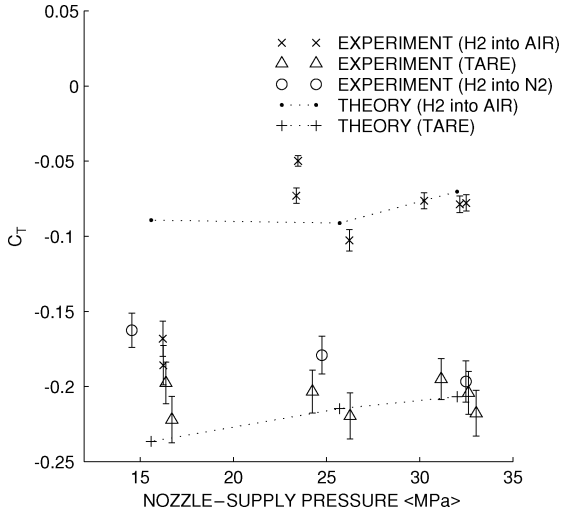


**Fig. 14 Coefficient of thrust at $\Phi = 0.80$ (nom.) for a range of nozzle-supply pressures (conditions 2D, 3G, and 4G).**

At least some of the scatter in the measured force coefficients can be attributed to variations in the equivalence ratios for the different conditions. The equivalence ratios for the results shown in Figs. 10 and 11 varied between 0.7 and 0.9. The only exception was the shot for hydrogen injection into a nitrogen flow at 3.6 MJ/kg, where the effective equivalence ratio was 1.0. Results from additional shots where the equivalence ratio was just outside the range 0.7 to 0.9 can be included, and the scatter in the results can be reduced by accounting for differences in the equivalence ratio.

The results in Figs. 6 and 7 indicate that the thrust and lift coefficients vary approximately linearly with equivalence ratio. This can be used to correct the measured coefficients to an equivalence ratio of 0.80. For example, consider a shot at an enthalpy of 4.0 MJ/kg that was performed with the aim of achieving an equivalence ratio of 0.80, but actually an equivalence ratio 0.95 was obtained. By fitting straight lines between the results for no injection and those at the measured equivalence ratio, it is possible to estimate the forces that need to be removed (or added) to account for the increase in equivalence ratio from 0.80 to 0.95. This procedure was applied to the measured data, and the results are shown in Figs. 12 and 13. The additional data, mainly around 3.3 MJ/kg, show good repeatability and the overall scatter in the results is reduced. Overall, good agreement is obtained between the theoretical and measured values. However, the measured lift coefficient does not increase as rapidly as indicated by the theoretical model.

### Variation of Static Pressure

Tests were performed to investigate the influence of variations in the freestream static pressure on the performance of the scramjet. Variations in freestream pressure were achieved by varying the nozzle-supply pressure from 16 to 32 MPa while keeping the nozzle-supply enthalpy fixed at nominally 3.3 MJ/kg. Shots with air as the test gas were done with fuel injection at $\Phi = 0.8 \pm 0.07$ and without fuel injection. Shots were also done with fuel injection into a nitrogen test flow.

The measured thrust coefficients are shown in Fig. 14. The thrust coefficients for the tare shots remained constant to within experimental uncertainty. There was a clear increase in thrust coefficient at the higher pressure conditions when fuel was injected into air. An increase in the lift coefficients was also obtained (see Fig. 15). The differences between these results and those for injection of hydrogen into a nitrogen test flow show the influence of combustion. For the 16-MPa condition there is little, if any, increase in thrust coefficient for the shots for fuel injection into air compared with those measured in the tare shots. Figure 15 shows that the measured lift coefficients for the low-pressure condition are also similar to the tare values. These results indicate that combustion heat release did not occur at the 16-MPa condition.

The theoretical thrust and lift coefficients are generally in good agreement with those measured. However for the tare conditions,

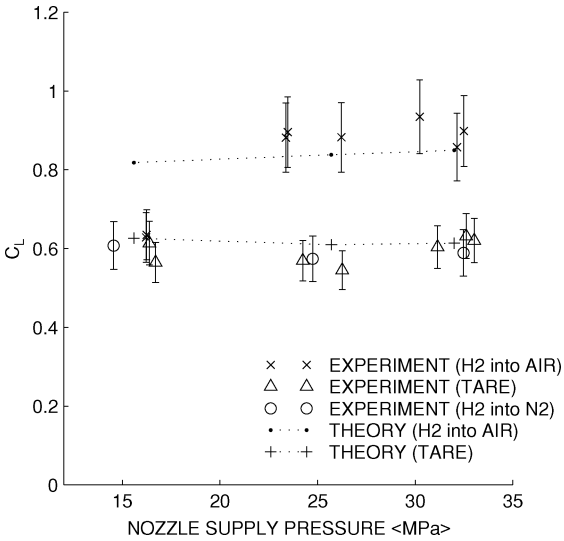


**Fig. 15 Coefficient of lift at $\Phi = 0.80$ (nom.) for a range of nozzle-supply pressures (conditions 2D, 3G, and 4G).**

the theoretical thrust coefficients are predicted to be lower at lower nozzle-supply pressures. This was not observed experimentally, and the agreement is poorest at the lowest pressure. This is attributed to the assumption of fully turbulent flow in the CFD components of the force predictions. At the 16-MPa nozzle-supply pressure condition, the Reynolds number is approximately half the value at the 32-MPa condition. Therefore, the contribution to the overall drag force from skin friction will be smaller at the lower-pressure condition if the boundary layer is laminar for a longer distance. The CFD calculations were run again for the 16-MPa condition, but boundary layers were set to be fully laminar. This resulted in a thrust coefficient of $-0.14$, compared to a fully turbulent value of $-0.24$. The measured thrust coefficients lie between these fully turbulent and fully laminar predictions, and so the differences between measurements and theory might be caused by the boundary layers undergoing transition in the scramjet.

Choking was evident in several shots at condition 4G in which fuel was injected into an air test flow. Choking causes flow in the combustion chamber to become subsonic and is characterized by strong shocks at the inlet, high pressures in the combustor, and high vehicle drag. Choking was identified in the experiments by a sudden jump in the pressures measured in the combustor and also by large lift and drag forces. The pressure measurements indicated that a normal shock wave formed first near the downstream end of the combustion chamber and that it moved upstream as the test progressed. The force balance indicated substantial changes in forces when the scramjet choked. When the duct choked at condition 4G, there was only a moderate increase in lift force, but the drag force increased by a factor of 2.5, and there was a change in sign of the moment coefficient. Although there was some degradation of the force signals when choking occurred, the results[31] indicated that the force balance still operated well when there was a large change in the distribution of loading on the model.

## Conclusions

A three-component force balance for the measurement of lift, thrust, and pitching moment on an operational model of a scramjet-powered vehicle was designed, built, calibrated, and tested. Experiments were performed to investigate the influences of variations in fuel mass flow rate, simulated flight altitude, and freestream pressure on performance of the vehicle.

This work has demonstrated that measurements of the overall performance of a model of an operational scramjet-powered vehicle can be made in a free-piston shock tunnel. This includes measurements of how much thrust can be developed, how the lift varies with engine operation and flight conditions, and how the engine operation alters the centre-of-pressure.

A large shift in center of pressure (up to 10%) was noted when the equivalence ratio varied from 0.0 to 1.0. Such a large change has important implications for the control of a scramjet vehicle. To compensate for this large shift in center of pressure, the control surfaces of the vehicle would need to be adjusted, and this would affect the other components of force acting on the model. The change in center of pressure was greatest at low equivalence ratios ($\Phi < 0.6$). This further highlights the importance of quantification of this parameter because relatively small changes in fuel flow rates produce large changes in the center of pressure.

The results show the importance of control of the combustor intake temperature and pressure. Thrust decreased with increasing nozzle-supply enthalpy. Also, there was no combustion when the pressure and temperature at entry to the burner were 50 kPa and 900 K, respectively. However, combustion did occur at a pressure and temperature 70 kPa and 900 K.

Choking of a scramjet engine will affect control of the vehicle. The drag of the present vehicle when the engine choked was approximately 2.5 times that with no fuel injection. A sign reversal in the pitching moment also occurred from a pitch-down to a pitch-up state.

A net positive thrust was not achieved even at the highest equivalence ratio tested. The modeling indicates that this was because of high skin-frictional forces (up to 50% of the total fuel-off drag) that acted on the model. Reduction of this drag is therefore critical to the successful development of a scramjet flight vehicle.

## Acknowledgments

This work was sponsored by a grant from the Australian Research Council. Robinson was support by an Australian Postgraduate Award. The authors would like to thank Scott Rowan, Myles Frost, Judy Odam, Rob Lowe, and Neil Griffiths for their assistance with the experiments.

## References

[1]Kors, D. L., "Design Considerations for Combined Air Breathing-Rocket Propulsion Systems," AIAA Paper 90-5216, Oct. 1990.

[2]Engelund, W. C., Holland, S. D., and Cockrell, J. C., "Propulsion System Airframe Integration Issues and Aerodynamic Database Development for the Hyper-X Flight Research Vehicle," *Proceedings of the 14th International Symposium on Airbreathing Engines*, ISOABE, Paper 99-7215, Sept. 1999.

[3]Gruber, M., Donbar, J., Jackson, K., Mathur, T., Baurle, R., Eklund, D., and Smith, C., "Newly Developed Direct-Connect High-Enthalpy Supersonic Combustion Research Facility," *Journal of Propulsion and Power*, Vol. 17, No. 6, 2001, pp. 1296–1304.

[4]Campbell, B. T., Siebenhaar, A., and Nguyen, T., "Strutjet Engine Performance," *Journal of Propulsion and Power*, Vol. 17, No. 6, 2001, pp. 1227–1232.

[5]Cockrell, C. E., Engelund, W. C., Bittner, R. D., Jentink, T. N., Dilley, A. D., and Frendi, A., "Integrated Aeropropulsive Computational Fluid Dynamics Methodology for the Hyper-X Flight Experiment," *Journal of Spacecraft and Rockets*, Vol. 38, No. 6, 2001, pp. 836–843.

[6]Billig, F. S., "Supersonic Combustion Ramjet Missile," *Journal of Propulsion and Power*, Vol. 11, No. 6, 1995, pp. 1139–1146.

[7]Rogers, R. C., and Capriotti, R. W., "Experimental Supersonic Combustion Research at NASA Langley," AIAA Paper 98-2506, June 1998.

[8]Mitani, T., Kanda, T., Hiraiwa, T., Igarashi, Y., and Nakahashi, K., "Drags in Scramjet Engine Testing: Experimental and Computational Fluid Dynamics Studies," *Journal of Propulsion and Power*, Vol. 15, No. 4, 1999, pp. 578–583.

[9]Kanda, T., Sunami, T., Tomioka, S., Tani, K., and Mitani, T., "Mach 8 Testing of a Scramjet Engine Model," *Journal of Propulsion and Power*, Vol. 17, No. 1, 2001, pp. 132–138.

[10]Kanda, T., Kouichiro, T., Kobayashi, K., Toshihito, S., and Sunami, T., "Mach 8 Testing of a Scramjet Engine with Ramp Compression," *Journal of Propulsion and Power*, Vol. 18, No. 2, 2002, pp. 417–423.

[11]Shimura, T., Sakuranaka, N., Sunami, T., and Tani, K., "Thrust, Lift and Pitching Moment of a Scramjet Engine," *Journal of Propulsion and Power*, Vol. 17, No. 3, 2001, pp. 617–621.

[12]Bernstein, L., "Force Measurement in Short-Duration Hypersonic Facilities," AGARDograph 214, Nov. 1975.

[13]Intrieri, P. F., Donn, B. K., Chapman, G. T., and Terry, J. E., "Ballistic Range Tests of Ablating and Non-Ablating Slender Cones," *AIAA Journal*, Vol. 8, No. 3, 1970, pp. 558–564.

[14]Bernstein, L., and Scott, G. T., "A Laser-Interferometric Trajectory-Following System for Determining Forces on Free Flying Models in a Shock Tunnel," *Proceedings of the 13th International Symposium on Shock Waves*, edited by C. E. Treanor and J. G. Hall, State Univ. of New York Press, Albany, NY, 1981, pp. 150–158.

[15]Naumann, K. W., Ende, H., Mathieu, G., and George, A., "Millisecond Aerodynamic Force Measurement with Side Jet Model in the ISL Shock Tunnel," *AIAA Journal*, Vol. 31, No. 6, 1993, pp. 1068–1074.

[16]Störkmann, V., Olivier, H., and Grönig, H., "Force Measurements in Hypersonic Impulse Facilities," *AIAA Journal*, Vol. 36, No. 3, 1998, pp. 342–348.

[17]Sanderson, S. R., and Simmons, J. M., "Drag Balance for Hypervelocity Impulse Facilities," *AIAA Journal*, Vol. 29, No. 12, 1991, pp. 2185–2191.

[18]Mee, D. J., Daniel, W. J. T., and Simmons, J. M., "Three-Component Force Balance for Fows of Millisecond Duration," *AIAA Journal*, Vol. 34, No. 3, 1996, pp. 590–595.

[19]Smith, A. L., Mee, D. J., Daniel, W. J. T., and Shimoda, T., "Design, Modelling and Analysis of a Six-Component Force Balance for Hypervelocity Wind Tunnel Testing," *Computers and Structures*, Vol. 79, No. 11, 2001, pp. 1077–1088.

[20]Paull, A., Stalker, R. J., and Mee, D. J., "Experiments on Supersonic Combustion Ramjet Propulsion in a Shock Tunnel," *Journal of Fluid Mechanics*, Vol. 296, 1995, pp. 159–183.

[21]Stalker, R. J., and Paull, A., "Experiments on Cruise Propulsion with a Hydrogen Scramjet," *The Aeronautical Journal*, Vol. 102, No. 1011, Jan. 1998, pp. 37–43.

[22]Robinson, M. J., Mee, D. J., Tsai, C. Y., and Bakos, R. J., "Measurement of Three Components of Force on a Large Scramjet in a Shock Tunnel," *Journal of Spacecraft and Rockets*, Vol. 41, No. 3, 2004, pp. 416–425.

[23]Takahashi, M., Komuro, K., Itoh, K. H. T., and Ueda, S., "Development of a New Force Measurement Method for Scramjet Testing in a High Enthalpy Shock Tunnel," AIAA Paper 99-4961, Nov. 1999.

[24]Mee, D. J., "Dynamic Calibration of Force Balances for Hypersonic Impulse Facilities," *Shock Waves*, Vol. 12, No. 6, 2003, pp. 443–455.

[25]Prost, R., and Goutte, R., "Discrete Constrained Iterative Deconvolution Algorithms with Optimized Rate Convergence," *Signal Processing*, Vol. 7, No. 3, 1984, pp. 209–230.

[26]Overton, S. C., and Mee, D. J., "T4's M5 and M8 Nozzle Pitot Rake Survey," *Proceedings of the 4th International Workshop on Shock Tube Technology*, edited by A. Paull, The Univ. of Queensland, Brisbane, Australia, Sept. 1994.

[27]McIntosh, M. K., "Computer Programmes for Supersonic Real Gas Dynamics," WRE-Technical Note 180, Australian Defence Scientific Service, Dec. 1970.

[28]Lordi, J. A., Mates, R. E., and Moselle, J. R., "Computer Program for the Numerical Solution of Nonequilibrium Expansions of Reacting Gas Mixtures," NASA, CR-472, May 1966.

[29]Krek, R. M., and Jacobs, P. A., "STN, Shock Tube and Nozzle Calculations for Equilibrium Air," Dept. of Mechanical Engineering, Rept. 2/93, Univ. of Queensland, Australia, Feb. 1993.

[30]Davies, W. R., and Bernstein, L., "Heat Transfer and Transition to Turbulence in the Shock Induced Boundary Layer on a Semi-Infinite Flat Plate," *Journal of Fluid Mechanics*, Vol. 36, 1969, pp. 87–112.

[31]Robinson, M. J., "Simultaneous Lift, Moment and Thrust Measurements on a Scramjet in Hypervelocity Flow," Ph.D. Dissertation, Dept. of Mechanical Engineering, Univ. of Queensland, Australia, Dec. 2003.

[32]Gardner, A. D., Paull, A., and McIntyre, T. J., "Upstream Porthole Injection in a 2-D Scramjet Model," *Shock Waves*, Vol. 11, No. 5, 2002, pp. 369–375.

[33]Smith, A. L., and Mee, D. J., "Dynamic Strain Measurement Using Piezoelectric Polymer film," *Journal of Strain Analysis for Engineering Design*, Vol. 31, No. 6, 1996, pp. 463–465.

[34]Daniel, W. J., and Mee, D. J., "Finite Element Modelling of a Three-Component Force Balance for Hypersonic Flows," *Computers and Structures*, Vol. 54, No. 1, 1995, pp. 35–48.

[35]Craddock, C., and Jacobs, P., "A Space Marching Compressible Flow Solver with Chemistry and Optimization," Dept. of Mechanical Engineering, Tech. Rept. 6/98, The Univ. of Queensland, Australia, 1998.

[36]Baldwin, B. S., and Lomax, H., "Thin Layer Approximation and Algebraic Model for Separated Turbulent Flows," AIAA Paper 78-257, Jan. 1978.

[37]Huber, P. W., Schexnayder, C. J. J., and McClinton, C. R., "Criteria for Self-Ignition of Supersonic Hydrogen-Air Mixtures," NASA TP 1457, Aug. 1979.

[38]Roache, P. J., "Perspective: A Method for Uniform Reporting of Grid Refinement Studies," *Journal of Fluids Engineering*, Vol. 116, March 1994, pp. 405–413.

[39]White, F. M., *Viscous Fluid Flow*, 2nd ed., McGraw–Hill, New York, 1991, Chap. 7.

[40]He, Y., and Morgan, R. G., "Transition of Compressible High Enthalpy Boundary Layer Flow over a Flat Plate," *Aeronautical Journal*, Vol. 98, No. 972, Feb. 1994, pp. 25–34.

[41]Spalding, D. B., and Chi, S. W., "The Drag of a Compressible Turbulent Boundary Layer on a Smooth Flat Plate with and Without Heat Transfer," *Journal of Fluid Mechanics*, Vol. 18, 1964, pp. 117–143.

[42]Goyne, C. P., Stalker, R. J., Paull, A., and Brescianini, C. P., "Hypervelocity Skin-Friction Reduction by Boundary-Layer Combustion of Hydrogen," *Journal of Spacecraft and Rockets*, Vol. 37, No. 6, 2000, pp. 740–746.